Nature of the ferroelectric phase transition in $PbTiO_3$

N. Sicron
Racah Institute of Physics, Hebrew University of Jerusalem, Jerusalem, Israel 91904

B. Ravel
Physics Department FM-15, University of Washington, Seattle, Washington 98195

Y. Yacoby
Racah Institute of Physics, Hebrew University of Jerusalem, Jerusalem, Israel 91904

E.A. Stern
Physics Department FM-15, University of Washington, Seattle, Washington 98195

F. Dogan
Department of Materials Science and Engineering FB-10, University of Washington, Seattle, Washington 98195

J.J. Rehr
Physics Department FM-15, University of Washington, Seattle, Washington 98195
(Received 1 September 1993; revised manuscript received 28 March 1994)

We have measured quantitatively the temperature dependence of the local distortions of $PbTiO_3$ crystals below and above the structural ferroelectric phase transition, using x-ray absorption fine-structure (XAFS) measurements. Two probe atoms, Pb and Ti, were used. The results were analyzed by fitting parametrized theoretical XAFS spectra to the experimental results. These measurements provide quantitative "distortion parameters" defined as the difference between the distance of the probe to its nearest neighbor measured in the actual structure and that in a centrosymmetric structure with the same unit cell dimensions. At low temperatures the Pb-edge spectra were fit using four shells and included single, double, and triple scattering configurations. The high-temperature fits included only two shells. The Ti-edge spectra were fitted with the first shell only. The Pb and Ti distortions vary relatively little with temperature below the transition and decrease faster near the transition temperature. Above the transition temperature, the Pb and Ti distortions at the peaks of their distortion distribution functions (DDF's) are both more than 70% of the corresponding low-temperature values. These results show that an essential element of order-disorder is present even in this nominally pure ferroelectric crystal which displays a soft mode and a dielectric constant typical of displacive-type ferroelectrics. The presence of the local distortions suggests that the displacements should have at least two correlation length scales, one associated with the the local distortions, the other with the order parameter.

I. INTRODUCTION

In materials undergoing structural phase transitions, the average distortion from the high-symmetry structure is represented by the order parameter. However, the actual local distortion can be quite different. One can consider two extreme cases. If the local distortions and the order parameter have similar temperature dependencies in a range including the transition temperature the transition is considered to be "displacive." On the other hand, if the size of the local distortions does not change with temperature across the transition, the transition is of the "order-disorder" type. In this case only the orientations of the local distortions change with temperature. Below the transition there is a preferred orientation. Above the transition the orientations are disordered. The distinction between the two is not absolute. Local distortions in a displacive crystal undergoing a second-order transition will not become zero just above the phase transition because of critical fluctuations. Similarly, the magnitude of the local distortions in an order-disorder crystal is never precisely constant because of elastic interactions. However, these two types of transitions involve different basic mechanisms. In the displacive case, an instability resulting from long range cooperative interactions produces the local distortions. In the order-disorder case the local distortions are due to local instabilities. Thus, it is of fundamental interest to our understanding of phase transitions to determine which mechanism dominates.

Perovskite crystals with an ABO_3-type molecular structure have long been considered as displacive type ferroelectrics.[1,2] The main evidence for this type of behavior has been the existence of a Brillouin zone center soft mode[3] both below and above the transition temperature and the large size of the dielectric con-

stant. Soft modes have been observed in many perovskite ferroelectrics.[4,5] In some the soft mode is underdamped even up to a few degrees from the transition temperature.[6,7] Excluding critical phenomena, the dielectric constant of crystals undergoing a second-order or weak first-order transition follows a Curie-Weiss law $\epsilon \propto \frac{C}{|T-T_c|}$ where T_c is the actual or extrapolated second-order phase transition temperature. It turns out that the proportionality constant C is much larger in displacive than in order-disorder-type ferroelectrics.[1] The coefficient C of perovskite crystals has values typical of displacive-type ferroelectrics. The existence of soft modes and the size of the dielectric constant led theoreticians to describe perovskite ferroelectrics as displacive.[3,8,9] According to these models, the atoms vibrate about center of inversion positions in the cubic phase. Below the transition temperature the structure distorts and the distortion increases with decreasing temperature.

During the last two decades much evidence accumulated indicating that local distortions in perovskite crystals also exist above the phase transition temperature.[10,11] The first to notice this were Comes *et al.*[12] They found diffuse x-ray lines above the transition temperature to the cubic phase indicating the existence of some form of structural disorder. Many types of optical experiments followed. These include Raman scattering,[13–16] hyper-Raman,[17] infrared reflectivity,[18] and optical refractive index.[19] These experiments show that local distortions are possibly present at temperatures far above the phase transition temperature. However, none of these experiments provide direct quantitative information on the magnitude and temperature dependence of these distortions. The first experiments to provide direct quantitative information on the temperature dependence of the distortions below and above the transition were x-ray Absorption Fine-Structure (XAFS) measurements[20] on $KTaO_3$:Nb crystals.[21–23] XAFS experiments showing disorder above the transition in mixed nonperovskite crystals were also reported.[24,25] XAFS measurements on $KNbO_3$ also indicate distortions above T_c but the results in this case were not analyzed in detail.[26] In the $KTaO_3$:Nb experiments, the positions of the Nb atoms were measured relative to the oxygen octahedra, to the K atoms at the corners of the cube and to the first Ta neighbors. The results show that the Nb atoms are displaced by about 0.145 Å in the [111] direction relative to the surrounding atoms. Furthermore, the magnitude of the displacements changes gradually by only 12% from about 16 K below the transition (T_c=85.6 K) to 215 K above it. These results show conclusively that the transition has at least partially an order-disorder character. Obviously, a pure order-disorder-type transition involving the Nb ions alone will not account for some of the experimentally observed features in this material such as the soft phonon[27] and a large inverse temperature coefficient of the dielectric constant.[28] It seems that, in this material, the host $KTaO_3$ provides a displacive component which, combined with the Nb ions, may account for the properties of this system. The question is what happens in a pure perovskite which has a very well-behaved soft mode and a large dielectric temperature coefficient characteristic of an ideal displacive ferroelectric. To answer this question we investigated $PbTiO_3$ which has been described as a classic case of a displacive ferroelectric.[1]

Above 763 K $PbTiO_3$ is cubic.[29] At this temperature it goes through a weak first-order transition to a tetragonal phase with a c/a ratio of 1.075 at 100 K.[30] In the tetragonal phase the crystal is ferroelectric. Both Pb and Ti atoms are displaced from their respective oxygen planes by 0.49 and 0.32 Å, respectively. The displacements are in the [001] direction. At ~183 K the crystal undergoes a transition to an orthorhombic phase with a very small change in the lattice parameters,[31] but remains ferroelectric. In addition an anomaly in the temperature dependence of the Pb displacement was observed at ~400 K. This anomaly is not accompanied by a visible change in the lattice parameters.[32]

A schematic representation of the low-temperature phase with the Pb and Ti atoms at the center is shown in Fig. 1. In the following we shall use the crystallographic notation and refer to the oxygens in the plane above and below the Pb as O_{2-} and O_{2+}, respectively, and the oxygens which are approximately in the Pb plane as O_1.

The soft modes of this material had been investigated by a number of groups as a function of temperature[6,33] and pressure.[7] The soft mode frequency decreases as the transition temperature is approached. It is underdamped at all temperatures and can be followed up to the first-order transition temperature[6] where its frequency is about 55 cm^{-1}. Near the transition temperature a central peak is observed.[34] The area of this peak seems to grow as the transition temperature is approached. This result is interpreted as a manifestation of some disorder present in the system close to the transition temperature on both sides. Furthermore, the dielectric constant in this material is found to be even larger than that expected from the Lydane-Sachs-Teller relation, suggesting that even the ordinary displacive-type model would not be sufficient to account for the dielectric constant. Fontana *et al.*[34] suggest that there is a crossover from displacive to order-disorder behavior near the phase transition temperature. Neutron diffraction experiments reported recently[35,36] also suggest that $PbTiO_3$ has a certain degree of disordered distortions above the phase transition. These results will be discussed in more detail in Sec. IV.

In this paper we report the temperature dependence of local distortions in $PbTiO_3$ obtained from (XAFS) measurements.[20,37,38] Previous XAFS measurements on $PbTiO_3$ have been reported but have not been analyzed in any detail.[39] XAFS is particularly suitable to provide quantitative local structural information for several reasons.[20] It can provide information on the structure surrounding different types of atoms in the system extending out to fourth-nearest neighbors providing the pair correlation function with very high resolution. In disordered systems it is better than any other presently available technique. It is not affected by long range orientational disorder and its effective measuring time is very short (on the order of 10^{-16} sec).

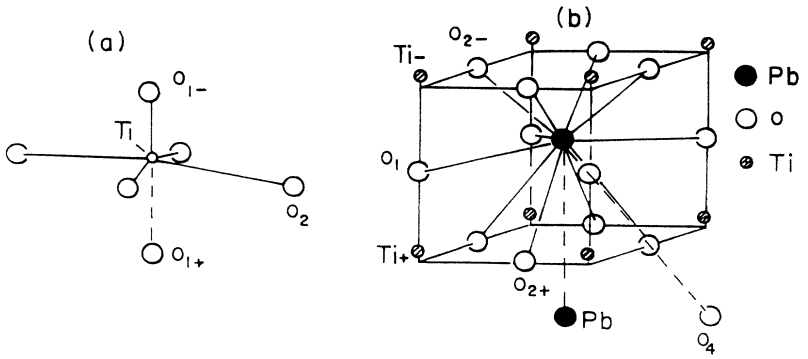

FIG. 1. Schematic structure of $PbTiO_3$ around each one of the probe atoms. (a) Ti, (b) Pb.

In this study, we used both Pb and Ti as probe atoms. The Pb XAFS provides us with the displacements of the Pb atoms relative to the oxygen octahedra and the Ti atoms. Analyzing the first shell of the Ti XAFS provides direct information on the Ti displacement relative to the oxygen octahedra. In addition, it provides direct information on the distortion of the oxygen octahedra themselves. Thus, the information obtained from the two probes is complementary.

Our results show that large local distortions exist even 190 K above T_c. Furthermore, the individual oxygen octahedra are tetragonally distorted also above T_c. But, in contrast to the $KTaO_3$:Nb case, the size of the distortion does decrease close to the phase transition.

In Sec. II we discuss the sample preparation and the XAFS experiments. In Sec. III we present the experimental results. The analysis of the results is described in Sec. IV and the physical meaning of the results is discussed in Sec. V. Section VI summarizes and concludes the paper.

II. SAMPLE PREPARATION AND EXPERIMENTAL CONSIDERATIONS

Pure lead titanate was prepared from an aqueous solution of nitrates of lead and titanium. The solution was coprecipitated by altering its pH with ammonia. The precipitate prepared in this fashion was a molecular mixture of lead and titanium. It was freeze dried then heat treated in air at 750 °C for 6 h. The resulting powder was checked by x-ray diffraction at room temperature to assure its crystal structure. It was found in the desired tetragonal phase. Scanning electron microscopy found that the typical dimension of the crystallites was of the order of a micron.

For the measurements on the lead L_{III} edge, the powder was mixed with graphite in proportions that assured an edge step of nearly unity.[20] Since the absorption length of the material is 11 μm at this edge and the material was well dispersed in the graphite, we were confident that thickness effects would not distort our data.[40] The graphite and $PbTiO_3$ mixture was dry pressed, producing a pellet that could be easily handled and placed within our experimental apparatus. The data for the lead edge XAFS were obtained in transmission at beamline X11-A at the National Synchrotron Light Source.

Transmission XAFS was not an option for the titanium edge measurements. The absorption length of the material at the Ti K edge is 2 μm. Since the crystallites were not small compared to this length, thickness effects would be introduced.[40] We therefore chose to prepare a sample for fluorescence. This was done by dry pressing the pure sample and sintering it at 1000 ° C for 30 min in ambient air. The final product was a yellow disk 15 mm in diameter and 1 mm thick. The fluorescence data were also collected at X11-A.

In both experiments a Si(111) double crystal monochromator in the nondispersive mode was used. The monochromator was detuned to 75% of the maximum intensity for harmonic rejection. This was particularly important for the titanium edge experiment because the rejected third harmonic could excite the lead L_{III} edge.

Care was taken at every stage of the experiment to avoid systematic distortions to the data. The sample was pure and homogeneous. A homogeneous spot in the beam was chosen and the width of the slits defining the beam was optimized for resolution. Gases were properly chosen for linear response in both detection chambers. The sample was repositioned in the beam frequently during the course of the experiment. This frequent realignment compensated for any changing conditions in the experiment or in the beam.

III. EXPERIMENTAL RESULTS

The Ti and Pb XAFS spectra were measured at 13 and 10 different temperatures, respectively, spanning the phase transition temperature. A large density of Ti XAFS measurements were done near the transition temperature. Examples of the extended XAFS spectra at several temperatures are shown in Figs. 2 and 3 for the Pb and Ti edges, respectively. For the sake of clarity, the spectra are presented after background removal, multiplied by the photoelectron wave number k, and as a function of k. The background removal and the determination of the threshold energies, E_0, are discussed in the next section. The important points to notice here are that the Pb spectra at low temperatures have a very good signal-to-noise ratio whereas the Ti data are noisy

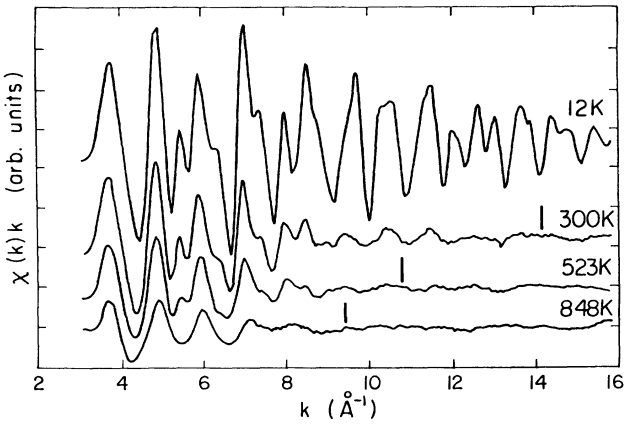

FIG. 2. The normalized Pb-edge XAFS multiplied by the photoelectron wave number k as a function of k for several representative temperatures. The vertical marks indicate the limits of useful XAFS data (see text).

even at room temperature. As the temperature increases the intensities of the Pb spectra decrease remarkably and the signal-to-noise ratio at large k decreases to a point where the data are no longer useful. The limits of the useful k range are indicated in Fig. 2. Except for changes in intensity the data do not display visible qualitative differences when going from temperatures far below to temperatures significantly above the phase transition.

IV. DATA ANALYSIS AND THE RESULTING STRUCTURAL PARAMETERS

A. Pb edge

The method of data analysis has been described by Mustre *et al.*[41,22] and by Hanske-Petitpierre *et al.*[23] The analysis is based on fitting the Fourier transforms of theoretical calculations to those of experimental spectra, in a specified range in r space, where r represents the distance to the probe. As a starting point for the theoretical calculation of the XAFS spectrum we used the room temperature structure of $PbTiO_3$.[36] Seen from the Pb probe (see Fig. 1), the first oxygen shell splits into three subshells with four oxygens each. The second, Ti, shell splits in two with four atoms each. The Pb shell splits into two subshells, one with two the other with four atoms. Finally, the fourth (oxygen) shell splits into four subshells. The basic model extends up to 5.38 Å from the probe and includes 51 atoms with 11 single, 34 double, and 14 triple different scattering paths. The theoretical XAFS spectrum was expressed in the following form:[41]

$$\chi(k) = \mathrm{Im}\sum_{\eta} n_\eta S_0^2 F_\eta(k) \times \exp\{i[kL_\eta + \Theta_\eta(k) - \tfrac{4}{3}k^3 C_{3\eta}]\} \times \exp(-2k^2\sigma_\eta^2). \quad (1)$$

Here the summation index η goes over all different scattering configurations; n is the number of equivalent paths, L is the path length, S_0^2 is an overall amplitude factor, σ^2 are the mean squared relative displacements, and C_3 is the third cumulant of the probability distribution function,[20] and is equal to the mean cubic relative displacement.

The scattering amplitude function $F(k)$ and phase shift $\Theta(k)$ were calculated by the *ab initio* FEFF5 code of Rehr *et al.*[44] These functions depend on the specific geometry of each configuration and on the participating atoms. In order to calculate the XAFS spectra for structures which differ slightly from each other we also calculated the first derivatives of the functions $F(k)$ and $\Theta(k)$ with respect to each one of the geometrical parameters that define the configuration. Using these functions our programs fit the XAFS spectra for any structure that does not deviate too strongly from the initial structure.[41] The distortions from the room temperature structure involved in the present problem are small enough for this purpose.

The model included four groups of parameters.

(a) Structural parameters. These include two tetragonal lattice parameters a and c and two distortion parameters d_{Pb} and d_{Ti} which measure the displacements of the Pb and Ti atoms, respectively, along the ⟨001⟩ direction. The first two parameters were not used as variable parameters in fitting theory to experiment. The Ti XAFS results discussed further down show that these values do not change significantly with temperature. Furthermore, the tetragonal distortion hardly affects the Pb-O and Pb-Ti distances. Thus, these values were taken as constants equal to their values at 150 K, namely, c=4.17 Å and a=3.90 Å. The other two parameters were the main objective of this work.

(b) The energy threshold E_0 and the overall amplitude S_0^2. E_0 is not determined by theory at this stage to better than a few eV; similarly S_0^2 can be off by ±15%. Therefore, both parameters are treated as variables and

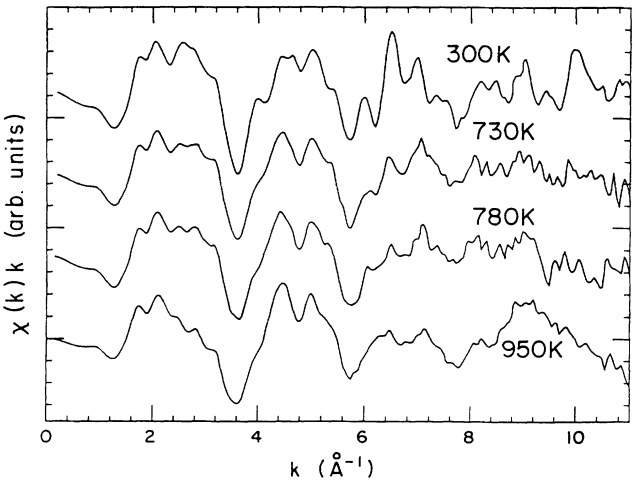

FIG. 3. The normalized Ti-edge XAFS absorption multiplied by the photoelectron wave number k as a function of k for several representative temperatures.

since they are temperature independent their values were adjusted so as to optimize the fits at all temperatures.

(c) Mean squared relative displacements (σ^2). The number of σ^2 parameters used at low and high temperatures was different. At the lowest temperature and up to room temperature four shells were fit and so we used six σ^2 parameters. One for the four nearest-neighbor oxygen bonds. Another for the other eight first shell oxygens. At high temperatures the total contribution of the more distant oxygens becomes small and the corresponding Debye-Waller factor is ill defined. Thus, we imposed the requirement that the ratio between the σ^2's of the short distance oxygens and the other oxygen subshells be constant and equal to the low temperatures (15–300 K) value, namely 0.78. This ratio is expected to be independent of temperature significantly above the Einstein temperature of the Pb-O bond. The Einstein temperature was found to be 252 K. Thus, the ratio obtained at room temperature is expected to remain constant at higher temperatures. Two additional σ^2 parameters were used for the two Ti subshells. Since the XAFS contributions of these shells extend over a relatively long range in k, the values of these parameters are well defined at all temperatures. Finally, for the third and fourth shells we used just one σ^2 parameter each. The third and fourth shells were fitted only at low temperatures. At high temperatures their contributions were too small to be used in the fitting process. The σ^2 parameters of the multiple scattering paths were estimated in terms of the previous parameters. In summary, when four shells were fit six σ^2's were used as variable parameters. At higher temperatures when only two shells were fit, three σ^2 parameters were used.

(d) Mean cubic relative displacements (C_3). This parameter reflects the anharmonicity in the relative vibrations between the probe and the neighboring atoms. It is expected to become non-negligible only at high temperatures. C_3 was used only for the closest oxygens. When used for Ti shells its value was negligible even at the highest temperatures.

The procedure for subtracting the background has been described in detail elsewhere[45] and will only be summarized here. In subtracting the background we used a spline with seven sections equally spaced in k space and with eight corresponding parameters. The spline was adjusted so as to minimize the difference between theory and experiment at the $r < 1.0$ Å region of the Fourier transform. The theoretical and experimental spectra were fit in the Fourier transform space. At low temperatures all four shells were used and the fit extended over $1.0 < r < 3.9$ Å range. At high temperatures only the first two shells were used and the fit extended over the range $1.0 < r < 3.6$ Å. For completeness the two-shell fit was also performed at low temperatures. The parameters obtained from the two types of fits were in good agreement with each other and varied much less than the experimental error.

The number of relevant independent experimental points $N \approx \frac{2\Delta k \Delta r}{\pi}$, where Δk and Δr are the k range with valid data and the fitting r range, respectively. As seen in Fig. 2, Δk decreases with rising temperature. For the four-shell model $N \approx 24$ and 20 at 12 and 300 K, respectively. For the two-shell model $N \approx 20$ and 10 at 12 and 848 K, respectively. The number of parameters used in the four-shell fit was nine and in the two-shell fit was six with two additional constant parameters which were the same in all fits. Thus, in both types of fit and at all temperatures the number of parameters was small compared to the number of relevant independent experimental points.

In Fig. 4 we show one example of the four-shell fit at 12 K and four examples of the two-shell fit. The contributions of certain shells and subshells to the theoretical spectrum at 12 K are shown in Fig. 5. All the subshell contributions of the first two shells are shown explicitly

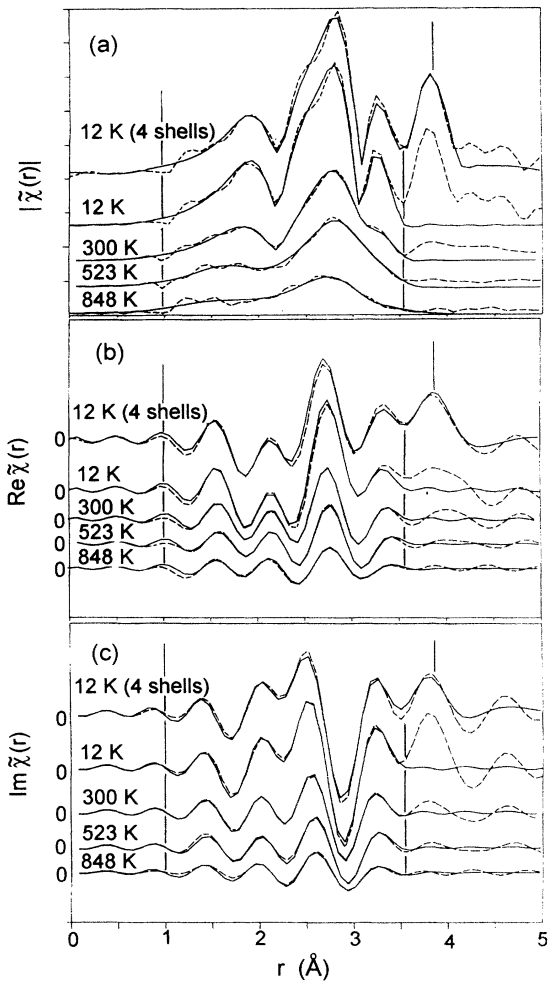

FIG. 4. The Fourier transforms of the Pb XAFS spectra $\tilde{\chi}(r)$ as a function of the distance to the probe r, for several representative temperatures. Dashed and solid lines represent the experimental results and the two-shell theoretical fits, respectively. (a) Absolute value, (b) real part, and (c) imaginary part. The temperatures are indicated in the figure. The vertical lines indicate the fitting ranges. Note that at 12 K both four- and two-shell fits are shown. The small difference between the two experimental curves is a result of a 1eV difference in E_0.

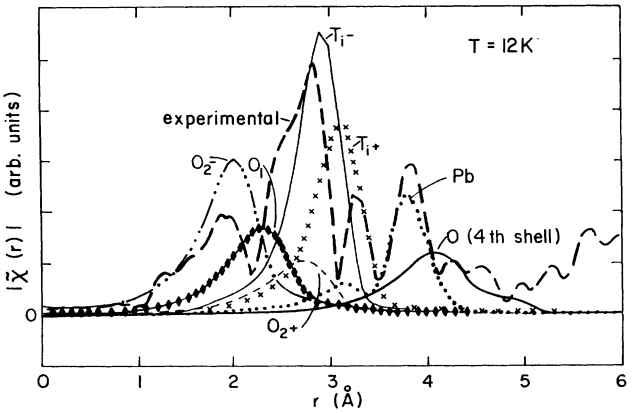

FIG. 5. The absolute values of the Fourier transforms of the 12 K Pb XAFS experimental spectrum and the contributions of various subshells and shells as a function of the distance to the probe r. The various contributions are indicated in the figure. O_{2-} and O_{2+} represent the short and long distance first-shell oxygens and O_1 represents the oxygens close to the Pb plane. Similarly Ti_- and Ti_+ represent the short and long distance titanium atoms. Pb and O represent the total single scattering contributions of the Pb and fourth-neighbor oxygens, respectively. (Notice that the theoretical contributions do not add up to the experiment result because these are absolute values.)

together with the contributions of the third and fourth shells. Note that the contributions are shown in absolute value. Thus, they do not add up to the absolute value of the experiment. It is clear from this figure, that the peaks, seen in the absolute value of the Fourier transform of the experimental spectrum, cannot be assigned to specific shells or subshells. However, it is seen that the contributions of the third and fourth shells are quite small below ~3.6 Å even at 12 K. At higher temperatures the relative contributions of these shells are even smaller. This fact enabled us to confine our analysis at high temperatures to the first two shells.

Finally, the energy threshold E_0 was found to be at the midpoint of the absorption step and S_0^2=0.93. The structural and σ^2 parameters are discussed in Sec. IV C.

B. Ti edge

Because the Ti-edge data were measured in the fluorescence mode, its quality was not as good as the Pb-edge data. However, the first shell is well separated from the more distant shells. These data were therefore analyzed only for the first shell and a simpler analysis procedure was adopted.

As a starting point for the theoretical calculation of the XAFS spectrum we used the room temperature structure of $PbTiO_3$.[42] Seen from the Ti probe (see Fig. 1), the first shell splits into three subshells. Two of the paths are to O_1 atoms lying along the c axis at distances of 2.39 and 1.77 Å from the Ti atom. The other four O_2 are in a plane perpendicular to the c axis. This plane is slightly offset from the midpoint between the O_1's in the c direction. The distance of these oxygens from the Ti probe is 1.97 Å.

The amplitude and phase functions $F(k)$ and $\Theta(k)$ were calculated using the *ab initio* FEFF5 code[44] and the theoretical XAFS spectrum was expressed in terms of six parameters. A single-energy threshold E_0, an overall amplitude factor S_0^2, a single σ^2 for all three oxygen subshells, and three additional structural parameters were used. These structural parameters were the distances of the Ti probe to the three oxygen subshells. From these distances one can calculate the a and c unit cell dimensions and the displacement of the Ti atom from the center of the octahedron. An attempt to use two σ^2's for the Ti-O bonds was made. The difference between the two

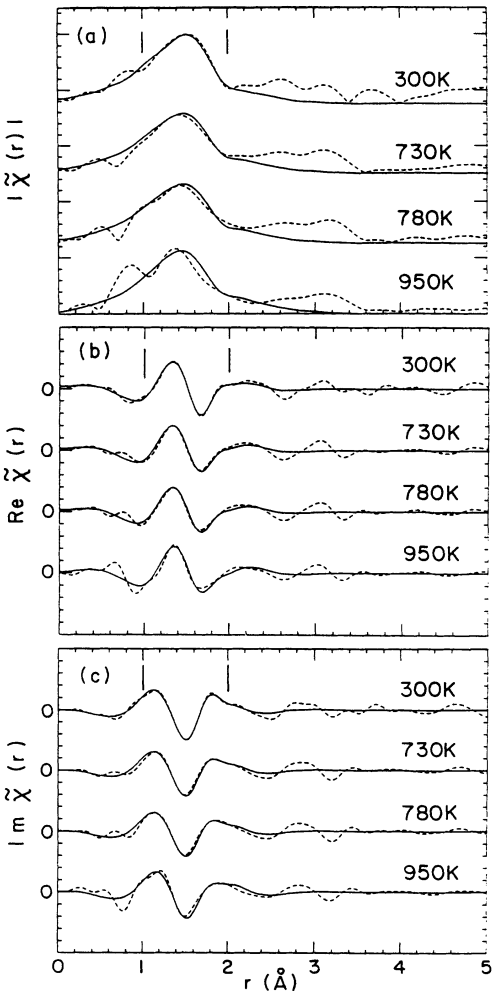

FIG. 6. The Fourier transforms of the Ti-edge XAFS spectra $\tilde{\chi}(r)$ as a function of the distance to the probe r, for several representative temperatures. Dashed and solid lines represent the experimental results and the theoretical fits, respectively. (a) Absolute value, (b) real part, and (c) imaginary part. The temperatures are indicated in the figure. The vertical lines indicate the fitting range.

was within the error brackets. An attempt to add a C_3 as in Eq. (1) did not yield any significant improvement in the fit nor did it significantly change the values of the other parameters.

The useful range in the photoelectron wave number k was 8.0 $Å^{-1}$. The Hanning window sills in k space were 2 $Å^{-1}$ wide and k^1 weighting was used. The fitting range in r space was from 1.0 to 2.2 Å. Using these ranges the number of relevant independent experimental points is about 7. Thus, using all six parameters as free variables would be a serious strain on the information content. In fact the model was not so seriously information limited. Two of the variables E_0 and S_0^2 are independent of temperature. Thus, at the end, a fixed value was used for each of these two parameters producing optimal fits to the spectra at all 13 temperatures. In the initial fits the σ^2 parameter was allowed to vary and the results were fitted to an Einstein model. In the final fits, the values obtained from the Einstein model were used as fixed σ^2 parameters. Thus in these fits we used three variable parameters at each temperature, namely the three additional structural parameters, and three parameters which were common and fixed at all temperatures.

The background from the experimental data was removed using the method described elsewhere.[45] The background spline function was characterized by seven parameters giving the spline values at seven equally spaced points in k space. The theoretical and experimental spectra were fit in r space using a Levenberg-Marquardt nonlinear least squares minimization. The Fourier transforms of the experimental and theoretical data are shown for several temperatures in Fig. 6. One sees that in this case the quality of background removal and the quality of the fits are not as good as in the Pb-edge data. We attribute this to the fact that the fluorescence data in this case are not as good as the transmission Pb-edge data. The error analysis includes the uncertainties introduced by the poorer quality of the data. The two nonstructural parameters found in this analysis are the energy threshold at 3.5 eV below the midpoint of the absorption step and the amplitude factor of 0.72 ± 0.04. Because the the fluorescence data were taken on a concentrated sample, this value must be corrected for self-absorption in the sample. This is a 15% effect, thus $S_0^2 = 0.83 \pm 0.05$. The structural parameters are discussed in the next subsection.

C. The mean squared relative displacements and the structural parameters

Before discussing the structural parameters obtained, we discuss error estimation. The errors have been carefully estimated using two different methods with comparable results. In these estimates, the effects of random experimental noise, and systematic experimental and theoretical errors have been included. Results of two different samples were analyzed and the parameter values agree better than the error brackets. A detailed discussion of the error estimation technique is available[46] and in UWXAFS 2.0 software documentation. In all the results reported below the systematic errors are dominant in determining the error brackets. Thus the scatter of the parameter values is small compared to the error brackets.

The temperature dependence of the Ti-O σ^2 is presented in Fig. 7. The experimental points were obtained when this parameter was allowed to vary. As mentioned before the final fits were done using the values on the Einstein curve. The σ^2's of the near oxygens and the two Ti subshells relative to the Pb probe are shown in Fig. 8. In all four examples the results are well fit with an Einstein model. The Pb-O_{2-} σ^2 is particularly large. This may be consistent with large Pb vibration amplitudes observed in neutron diffraction.[35]

The temperature dependence of the third cumulant, C_3, of the Pb-O_{2-} bond is presented in Fig. 9. Up to 300 K this parameter is negligible, but as the temperature increases further, it increases (within the error brackets) as T^2.[47] This parameter reflects the anharmonicity of the Pb-O_{2-} vibrations and therefore the asymmetric character of the Pb-O_{2-} distance distribution function. This function was calculated using the three lowest cumulants obtained in the fit: the mean Pb-O_{2-} distance, σ^2 and C_3. The results for various temperatures are presented in Fig. 10. We define the distortion distribution function as the distance distribution function with the abscissa equal to half of the diagonal distance between O_{2-} and O_{2+} minus the Pb-O_{2-} distance (see upper scale in Fig. 10). At low temperatures the function is symmetric. As the temperature increases the function becomes asymmetric. The function is much steeper at the short distance side and as the temperature rises the peak moves towards smaller distortions.

The temperature dependence of the local unit cell dimensions are shown in Fig. 11. The c dimension is equal to the sum of the Ti to oxygen distances along the c direction and the a dimension can be calculated from the Ti to O_2 distance taking into account the displacement of the Ti in the c direction. Also shown by circles are the geometric average of the local cell dimensions, given

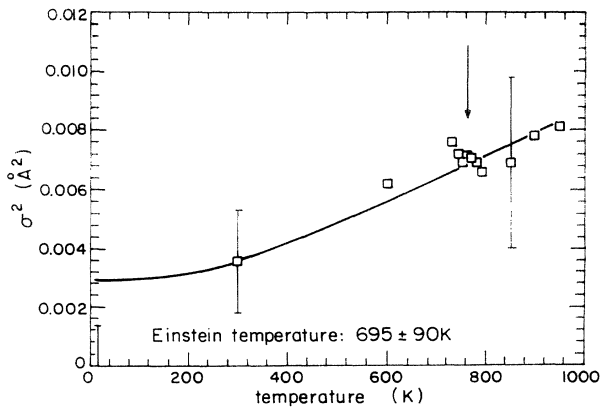

FIG. 7. The temperature dependence of the σ^2 of the Ti to oxygen bond. They were obtained when this parameter was allowed to vary. The solid line is an Einstein fit to the experimental points. The transition temperature is indicated by the arrow.

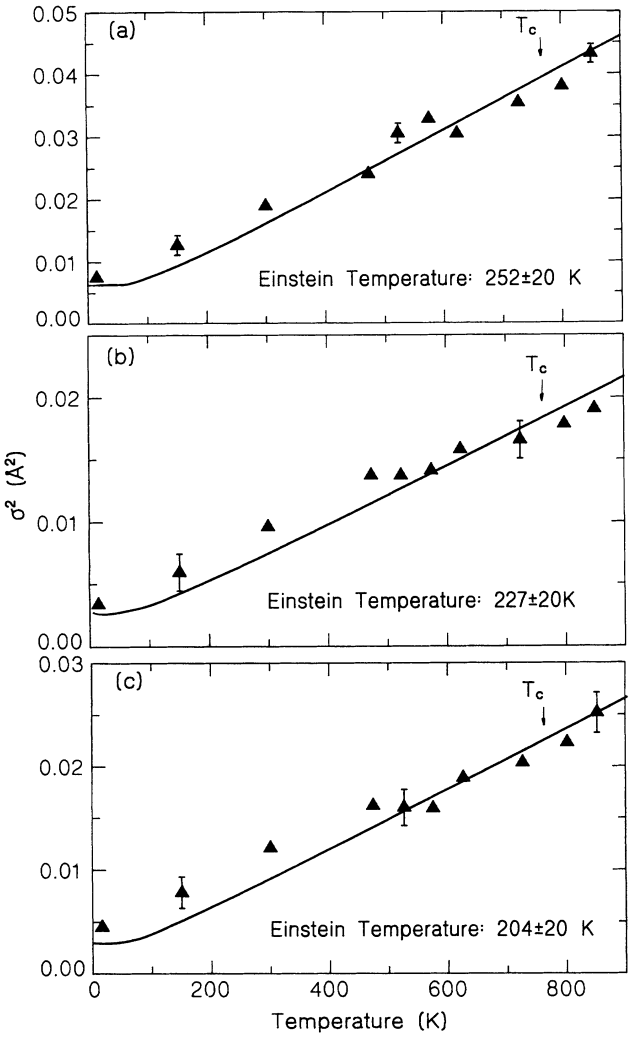

FIG. 8. The temperature dependence of Pb edge σ^2's. The solid △'s represent the experimental results. The solid lines are Einstein model fits to the data. The Einstein temperatures obtained are shown in the figures. (a) σ^2's of the Pb to near oxygen bond. (b) σ^2's of the Pb to near Ti bond. (c) σ^2's of the Pb to far Ti bond.

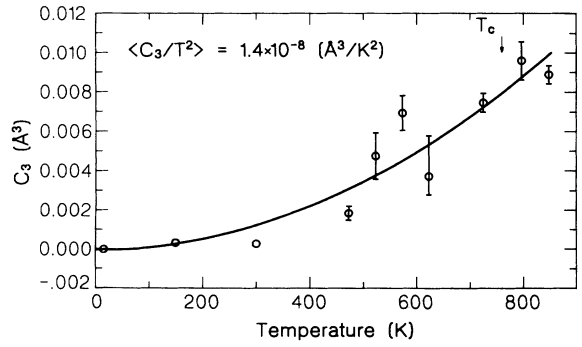

FIG. 9. The temperature dependence of the Pb to nearest oxygen third cumulant, C_3. The solid line represents a T^2 fit.

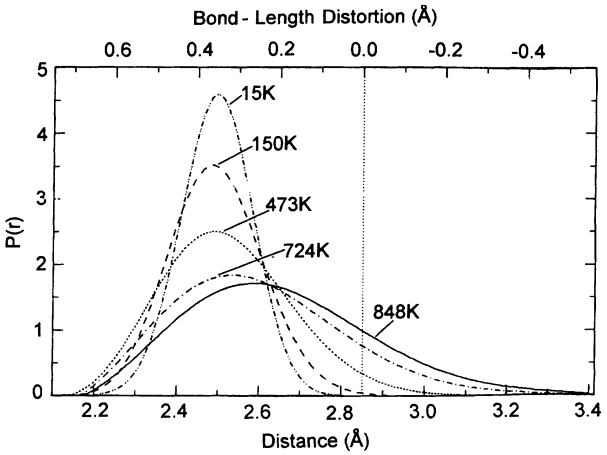

FIG. 10. The calculated Pb to nearest oxygen distance distribution function (DDF) at various temperatures. The vertical line indicates half the diagonal distance between O_{2-} and O_{2+}. The upper scale is the distortion. Notice that the shortest Pb-O_{2-} distance reaches a minimum value at 150 K and remains almost constant all the way to 848 K.

by $(a^2c)^{\frac{1}{3}}$. The results are quite surprising because they show that the cells are strongly distorted even far above the transition temperature. In fact the local tetragonal distortion changes by only ~15% from 12 to 950 K. This in itself shows that the local structure above the transition differs significantly from the cubic structure. The fact that in the cubic phase the cells are locally tetragonal and the structure on the average is cubic suggests that the crystal consists of correlated nanoregions of distorted cells with different distortion orientations.

The error bars shown are much larger than the random fluctuations of the data points, reflecting the fact that the errors are dominated by systematic effects. The relative variation of the data is more reliable than indicated by the error bars. In Fig. 11 the average of the local cell di-

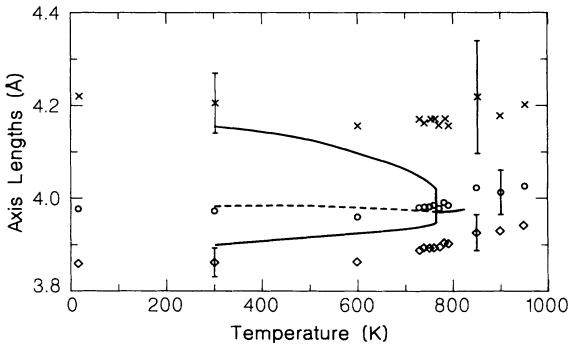

FIG. 11. Temperature dependence of the a and c unit cell dimensions. Solid lines represent the average dimensions obtained from x-ray diffraction (Ref. 30). The dashed line represents the geometric average of the lattice constants. The x's and diamonds represent the c and a axes obtained from the Ti-edge XAFS. The circles are the average lattice constants above T_c as obtained from the XAFS results by $(a^2c)^{\frac{1}{3}}$.

mensions is consistent, within the uncertainties, with the average structure measured by diffraction. These agreements verify the accuracy of the XAFS results.

The average Pb distortion and the distortion at the peak of the distortion distribution function, DDF, are shown in Fig. 12. Notice that at low temperatures the XAFS results are slightly larger than the x-ray[32,30] and neutron diffraction[36] results. However at higher temperatures the distortions obtained from x-ray diffraction fall off roughly as $(T-T_c)^{1/2}$. The results obtained from neutron diffraction are systematically larger and are nonzero even above the phase transition. These results were analyzed allowing for disorder in the Pb positions similar to the distortions present below the transition temperature. The average distortions obtained from XAFS follow the neutron diffraction results below T_c but above T_c they are slightly larger and are about 50% of the value at 12 K. The distortions at the peaks of the DDF remain constant almost all the way to T_c. Above T_c they are larger than the mean distortions by 0.08 Å and are more than 70% of the peak distortion at 12 K.

The displacement of Pb along the c axis can be calculated from the Pb distortions by taking its component along the c direction. The average displacements calculated are 0.53, 0.48, and 0.27 Å at 12, 473, and 848 K, respectively. The calculated displacements above ~500 K are only estimates because the Pb and O_2 vibrations may be correlated producing a larger displacement than the one calculated here. For this reason we display the distortions as defined above rather than the displacements along the c direction.

The temperature dependence of the lead to the near titanium distance is shown in Fig. 13. Within the experimental error this distance does not change with temperature. It corresponds to a 0.16(.03) Å vertical displacement of the Ti atoms from the center of the Pb cube. The displacement of the Ti atoms from the center point between the O_1 oxygens as measured from Ti-edge XAFS is presented in Fig. 14. This displacement can also be

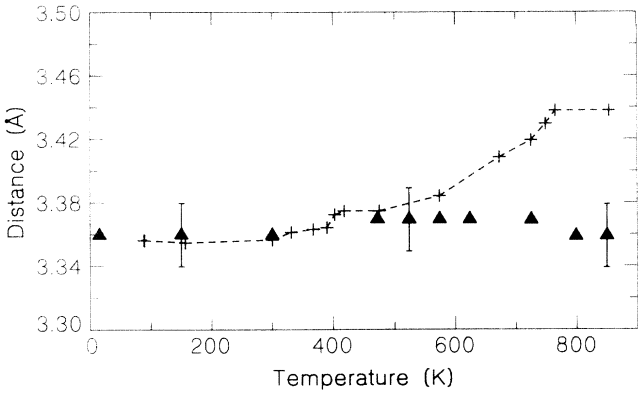

FIG. 13. The temperature dependence of the Pb to near Ti distance. +'s represent x-ray data (Refs. 32 and 42) and Solid △'s, the results obtained from Pb-edge XAFS.

calculated from the Pb-edge XAFS using the Pb-Ti and Pb-O_2 distances. At low temperatures the two values match but as temperature increases the Pb edge value is considerably smaller than the Ti-edge result. The reason for this mismatch is that at high temperatures the vibrations are large as can be seen in Fig. 8. If correlations are important the Ti displacement can not be reliably calculated from the Pb-edge XAFS. One possible scenario is the following: Suppose at high temperature the Pb vibration in the z direction is large and correlated with the O_2 displacement in the (xy) plane. Then when the Pb moves closer the oxygens move away to make room. In this case the actual average Pb displacement in the z direction will be larger than the one we calculate. This will account for the smaller calculated Ti displacement. The results in Fig. 14 show that the displacement of the Ti atoms from the center point between the O_1's changes only little below the transition temperature. It then decreases faster in the vicinity of the transition and remains clearly nonzero above the transition temperature. The

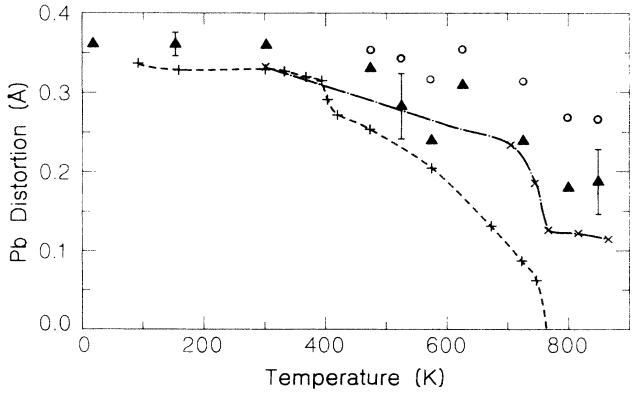

FIG. 12. The temperature dependence of the Pb distortion. The open circles indicate the distortion calculated from the peak of the DDF. The solid △'s are the average distortions obtained from the Pb-edge XAFS data, the +'s are from x-ray diffraction (Refs. 32 and 42), and the x's are from neutron diffraction (Ref. 36).

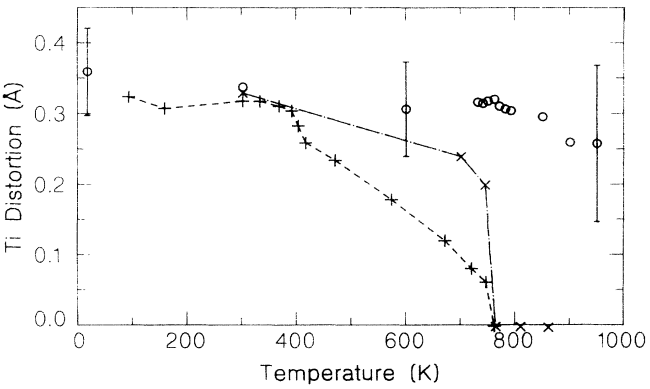

FIG. 14. The displacement of Ti from the midpoint between the two O_1 planes. +'s and ×'s represent the x-ray (Refs. 32 and 42) and neutron diffraction (Ref. 36) results, respectively. Open ○'s represent the results obtained from Ti XAFS.

displacement at 950 K is still about 70% of the displacement at 12 K. The results of the x-ray[42,32] and neutron measurements[36] are also displayed in Fig. 14. The neutron diffraction and Ti XAFS results agree fairly well below the transition temperature. However above the transition the neutron results suggest that the Ti goes back on center in contrast to the results of both the Pb and Ti XAFS.

The fact that the local distortions are nonzero above the transition while the order parameter is zero shows that the distortions must have orientational disorder. Partial disorder must be present also below the transition because the local distortions are larger than the average. However since the Pb data can be fitted with just two Ti subshells at all temperatures, the displacements of neighboring Ti and Pb atoms must remain correlated over at least several unit cells. If the displacements of Pb and Ti were not correlated at least four Pb-Ti distances would be needed to fit the data.

Several steps have been taken to verify that a local cubic symmetric structure contradicts the XAFS data above T_c. We calculated directly the theoretical Pb XAFS spectra using the cubic structure with the x-ray determined unit cell ($a = c = 3.97$ Å) as a starting point. We then used four variable parameters: E_0, the σ^2's of Pb-O and Pb-Ti, and a Ti phase shift correction. The fit results at the highest temperature are shown in Fig. 15 in comparison with the fit of the distorted structure. The fit was performed in the range $3 < k < 10.5$ Å^{-1}. As mentioned above, there is no signal above $k = 10$ Å^{-1}. The fit of the cubic model is clearly much worse. The least sum of squares in the cubic fit is five times worse than the corresponding value for the tetragonal fit. When we allowed the distortion parameters to vary, they converged within the experimental error to the values we found previously. A similar test was performed on the Ti-edge XAFS. The results are shown in Fig. 16. The fit to the cubic model is two times worse than to the distorted model and the fact that the latter had one additional variable parameter cannot by itself account for this improvement.

We also checked the eight-site model for the Ti displacements above T_c and verified that it contradicts the XAFS data. Self-consistent total energy calculations within the local density approximation for $PbTiO_3$ indicate that the large tetragonal strain in the ferroelectric phase stabilizes the tetragonal structure.[43] Above T_c where no long range tetragonal strain exists, the calculation suggests that the Ti atoms will randomly displace along the eight ⟨111⟩ directions rather than the six ⟨001⟩ directions. A fit to the Ti-edge data above T_c was performed assuming the eight-site model. In this case symmetry requires that the six oxygen backscattering paths split into two groups of three paths. These path lengths can be parametrized by a single parameter, δr, which defines the displacement from the cell center in a ⟨111⟩ direction. In this model the fit is 1.5 times worse than that of the tetragonal model. The result of this fit is shown in Fig. 16(c) and as can be seen the tetragonal fit is much better than the eight-site model.

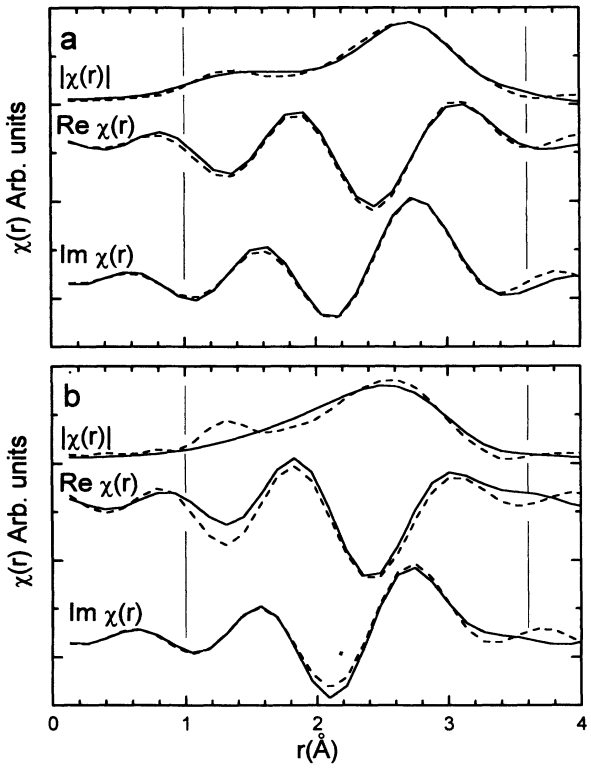

FIG. 15. The fit of theory (solid line) and experiment (dashed line) of the absolute, real, and imaginary spectra of the Fourier transforms of the Pb-edge XAFS results at 848 K. (a) The distorted model. (b) The cubic model. The vertical lines represent the fitting range. The two experimental curves are a little different because E_0 was allowed to vary in the cubic fit in order to optimize it. Notice that the distorted model fits the experimental results much better than the cubic one.

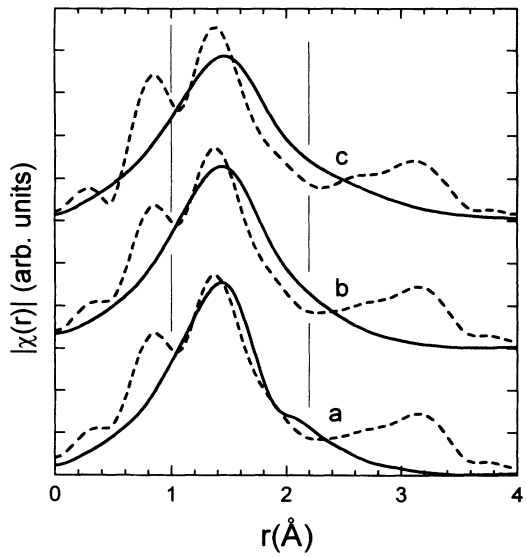

FIG. 16. The fit of theory (solid line) and experiment (dashed line) of the absolute value of the Fourier transforms of the Ti-edge XAFS results at 950 K. (a) The tetragonally distorted model, (b) the cubic model, and (c) the eight-site model. The vertical lines represent the fitting range. Notice that the tetragonally distorted model fits the experimental results much better than the others.

V. DISCUSSION

It is important to understand the differences among the results obtained from x-ray diffraction, neutron diffraction, and XAFS. As long as some long range order is present, diffraction spectra are essentially composed of δ functions, even if structural disorder is present. In this case there is also a weak broad background which is usually ignored. The disorder does however affect the relative integrated intensities of the various δ functions. Thus in principle, the spectra do contain information on the disordered structural distortions. To obtain this information it is necessary to introduce the disordered distortions to the fit model and to have sufficient range in k space in order to resolve the disordered distortions. Since disordered distortions were not taken into account in most x-ray models, these experiments provided information only about the average structure. In this case local distortions show up only as inflated Debye-Waller factors. In analyzing the neutron diffraction results local distortions were taken into account and such distortions were detected in the paraelectric phase.[36] However, the quantitative accuracy of the results is inferior to that of XAFS. In neutron diffraction[36] the range of momentum transfer used in this case was about 9 Å^{-1} and, as pointed by the authors, it is difficult to distinguish between a large anharmonic mean thermal amplitude and disordered displacements. XAFS is in a better state to distinguish the two apart because the corresponding momentum range is between 32 and 21 Å^{-1}, two times the maximum photoelectron wave number at 12 and 950 K, respectively.

In the present case XAFS was able to provide both average distortions and σ^2's. The average local distortions of Pb and Ti at ~800 K are 0.18 and 0.20 Å, respectively. The value of the σ of the Ti-O bonds is ~ 0.12 Å. In the case of Pb the width of the DDF can be determined visually from Fig. 10. It is found that above T_c the DDF falls to half of its maximum value at zero distortion. Thus, the DDF's of Ti and Pb are clearly different from a broad distribution with a maximum at zero which would be generally expected for a simple displacive transition.

This result has two important consequences. First, the local distortions cannot be a result of defect or surface strains. Such effects would tend to smear the distribution function. Also, the defect and surface effects observed so far have been strongly temperature dependent and showed up only close to T_c in contrast to present results. Second, it seems that the local distortions are a result of local instabilities rather than the ferroelectric phase transition. This behavior has been observed in a more pronounced way in $KTaO_3$:Nb. In that case the Nb displacements were almost independent of temperature and Nb concentration indicating that the Nb displacements takes place whether the system undergoes a phase transition or not.

The Pb-O_{2-} distribution function shown in Fig. 10 displays one very interesting feature. In spite of the fact that the width of the distribution function grows strongly with temperature the minimum Pb-O_{2-} distance does not change above 150 K. This means that at this distance the repulsion between the two grows very steeply. This further suggests that the displacement of the Pb towards the center may be due simply to the increase in the vibrational amplitude combined with the wall-like repulsion from the nearest oxygen.

The temperature dependence of the local distortions suggests the following qualitative picture. At very low temperatures the crystal is uniformly distorted and the local and average distortions are equal to each other. As the temperature rises clusters with different polarization orientations form. Their number and volumes grow while the polarization per unit cell may somewhat decrease. Thus, the local distortions decrease much less than the average polarization. Above the transition, the local distortion, at the peak of the distortion distribution function, is smaller but well above zero and the contributions of the different types of clusters average out to zero. The polarization autocorrelation function is expected to have at least two length scales. One is related to the cluster sizes, the other to the correlation of the order parameter. The latter scale would be large compared to the cluster size below and, at least, in the vicinity above T_c, and would grow critically as the transition temperature is approached. The XAFS results provide direct information that the length scales of the cluster sizes extend to at least a few unit cells at all temperatures measured.

Our results indicate that locally little happens as the long range order disappears above T_c. The local distortions change only slightly and the correlations between the displacements in neighboring cells remain about the same. If the range of interactions between atoms that causes the local instability is smaller or of the order of the cluster size, then one can understand why the local structure changes only slightly above T_c. These results agree with the theoretical calculations for $PbTiO_3$ that predict that the ferroelectric transition has an essential order-disorder element,[43,11] as local displacements remain above T_c. However we do not find the predicted[43] change in the displacements from tetragonal to rhombohedral above T_c. The persistence of the tetragonal displacement is indicative that the range of the interaction causing the instability is smaller than the cluster size.

Soft modes and central peaks are measured at a well-defined point in the reciprocal space of the crystal. The linear dimension of reciprocal space involved is usually only about 1×10^{-4} to 1×10^{-2} of the linear size of the Brillouin zone. This corresponds to a correlation length of 10^2–10^4 unit cells in real space. In contrast the linear size of the clusters in real space is expected to be much smaller, corresponding to a much larger fraction of the Brillouin zone. Thus, soft modes can coexist with local distortions and the temperature dependencies and origin of central peaks, observed by diffraction and light scattering techniques, can be different from those of the local distortions measured by XAFS.

The fact that the lattice is clearly distorted locally above T_c for at least as high as 190 K above the transition temperature and the fact that the distortions there are more than 70% of the distortions at 12 K, clearly

show that this system can by no means be described as a classic displacive ferroelectric. Any microscopic theory discussing the ferroelectric phase transition must either explain or at least take these facts into account. However, it should be equally emphasized that $PbTiO_3$ cannot be described as a pure order-disorder ferroelectric either for several reasons. First, the local distortions do change near T_c. Second, $PbTiO_3$ displays a clear underdamped zone center soft mode both below and above the transition temperature. Third, as mentioned above the proportionality constant relating the dielectric susceptibility and $(T - T_c)$ of an order-disorder ferroelectric is about 1 to 2 orders of magnitude smaller than that of displacive ferroelectrics. In $PbTiO_3$ the experimental coefficient is even larger than that calculated for a purely displacive transition from the Lydane-Sachs-Teller relation.[34] Thus, neither a pure displacive nor a pure order-disorder theory is sufficient to describe the properties of $PbTiO_3$.

VI. SUMMARY AND CONCLUSIONS

In this paper we presented the XAFS spectra of $PbTiO_3$ measured at various temperatures both below and above the ferroelectric phase transition. Both Ti and Pb x-ray absorption edges were used. The spectra were analyzed in detail by fitting theoretical calculations to the experimentally measured XAFS spectra. The low-temperature Pb-edge XAFS were fit up to a distance of 3.9 Å using four shells. The theoretical model included contributions from single and multiple scattering configurations. At high temperatures only two shells were included because the contributions of the other two shells were too small and too noisy to be useful. The Ti-edge fluorescence XAFS spectra were noisier than the Pb spectra and were therefore analyzed for the first shell only. Yet, the Ti analysis provided important information on the temperature dependence of the local unit cell structure and the Ti off-center displacement.

Direct quantitative information on the local structure surrounding both probes was obtained and it can be summarized as follows.

(1) Locally unit cells remain tetragonal even above the transition temperature with the cell distortions from the cubic structure changing by less than 15% over the entire temperature range.

(2) The Pb atoms are displaced from the corresponding oxygen planes of the ideal perovskite structure in the [001] direction both below and above the phase transition temperature. The distortion distribution function (DDF) is symmetric and off center at low temperatures. As the temperature rises the distribution function broadens asymmetrically leaving the shortest Pb oxygen distance constant. The peak of the distribution moves to smaller values but remain at 75% of the value at low temperatures even at the end of the measurement range, 85 K above the transition temperature.

(3) The Ti atoms are displaced from the center of the Pb cubes. Within the experimental error these displacements are independent of temperature.

(4) The Ti-edge XAFS show that the Ti atoms are displaced relative to the oxygen octahedra both below and above the transition temperature. The displacement varies little below the transition, more rapidly close to the transition and saturates at a value of about 70% from the low-temperature value at least up to the end of the experimental temperature range, 190 K above the transition.

(5) Above T_c the tetragonal distortions remain well correlated in neighboring cells and this correlation extends a finite length producing a cluster which is larger than the range of the interaction that causes the instability.

The results show that the DDF's of both Pb and Ti have well-defined peaks at off zero displacements even above T_c. The fact that the peaks are well defined implies that the local distortions are not a result of defects or strained surfaces. Furthermore, the microscopic mechanism creating the distortions is local instabilities rather than long range cooperative interactions.

In summary we are led to the conclusion that even a pure perovskite like $PbTiO_3$ which was considered to be an exemplary displacive ferroelectric is by no means purely displacive. The fact that both Pb and Ti atoms are displaced from their corresponding center of inversion positions well above the transition temperature shows that the system is clearly disordered but the fact that the magnitude of these displacements is affected by the phase transition shows that the displacive nature of the transition cannot be ignored either.

The observation of local distortions above T_c poses the question whether all structural phase transitions have a necessary requirement of a local instability. If this is the case then all such transitions have an essential element of order-disorder with a possible enhancement of the local distortions by long range interactions. The fact that even a classic example of a displacive transition still shows a large remnant local distortion above the transition lends much weight in favor of this speculation.

ACKNOWLEDGMENTS

This work was supported in part by DOE Grant No. DE-FG06-90ER45425 and BSF Grant No. 92-00348. Beamline X11-A is supported by DOE Grant No. DE-FG05-89ER45384. We wish to thank M. Newville and Y. Zhang for their assistance in collecting data and Dr. R. Cohen, Professor. I. Bersuker, Professor D. Thouless, and Professor B. Spivak for stimulating discussion.

[1] M.E. Lines and A.M. Glass, *Principles and Applications of Ferroelectrics and Related Materials* (Clarendon Press, Oxford, 1977).
[2] R. Blinc and B. Zeks, *Soft Modes in Ferroelectrics and Antiferroelectrics* (Elsevier, New York, 1974).
[3] W. Cochran, Adv. Phys. **9**, 387 (1960).
[4] J.F. Scott, Rev. Mod. Phys. **46**, 83 (1974).
[5] J.D. Axe, J. Harada, and G. Shirane, Phys. Rev. **B 1**, 1227 (1970).
[6] G. Burns and B.A. Scott, Phys. Rev. **B 7**, 3088 (1973).
[7] J.A. Sanjurjo, E. Lopez-Cruz, and G. Burns, Phys. Rev. **B 28**, 7260 (1983).
[8] E. Pytte and J. Feder, Phys. Rev. **187**, 1077 (1969).
[9] R. Migoni, H. Bilz, and D. Bauerle, Phys. Rev. Lett. **37**, 1155 (1976).
[10] B.E. Vugmeister and M.D. Glinchuk, Rev. Mod. Phys. **62**, 933 (1990).
[11] I.B. Bersuker and V.Z. Polinger, *Vibronic Interactions in Molecules and Crystals*, edited by V.I. Goldanski, Springer Series in Chemical Physics Vol. **49** (Springer-Verlag, New York, 1989).
[12] R. Comes, M. Lambert, and A. Guinier, Solid State Commun. **6**, 715 (1968).
[13] A.M. Guitet, M. Lambert, and A. Guinier, Solid State Commun. **12**, 1053 (1973).
[14] Y. Yacoby and S. Just, Solid State Commun. **15**, 715 (1974).
[15] Y. Yacoby, Z. Phys. B **31**, 275 (1978).
[16] Y. Yacoby, Z. Phys. B **41**, 269 (1981).
[17] H. Vogt and H. Uwe, Phys. Rev. **B 29**, 1030 (1984).
[18] F. Gervais, Ferroelectrics **53**, 91 (1984).
[19] G. Burns and F. Dacol, Ferroelectrics **37**, 661 (1981).
[20] E.A. Stern and S.M. Heald, in *Handbook of Synchrotron Radiation*, edited by E.E. Koch (North-Holland, Amsterdam, 1983), Vol. 1, Chap. 10, p. 955.
[21] O. Hanske-Petitpierre, E.A. Stern, and Y. Yacoby, J. Phys. C **8**, 675 (1986).
[22] J. Mustre, Y. Yacoby, E.A. Stern, J.J. Rehr, and M. Dell'ariccia, Physica **B 158**, 263 (1989).
[23] O. Hanske-Petitpierre, Y. Yacoby, J. Mustre-deLeon, E.A. Stern, and J.J. Rehr, Phys. Rev. **B 44**, 6700 (1991).
[24] Q.T. Islam and B.A. Bunker, Phys. Rev. Lett. **59**, 2701 (1987).
[25] Z. Wang and B.A. Bunker, Phys. Rev. **B 46**, 11277 (1992).
[26] K.H. Kim, W.T. Elam, and E.F. Skelton, *Optical Fiber Materials and Processing*, edited by J.F. Fleming *et al.*, MRS Symposia Proceedings No. **172** (Materials Research Society, Pittsburgh, 1990), p. 291.
[27] S.K. Manlief and H.Y. Fan, Phys. Rev. **5**, 4046 (1972).
[28] D. Rytz, U.T. Höchli, and H. Bilz, Phys. Rev. **B 22**, 359 (1980).
[29] G. Shirane and S. Hoshino, J. Phys. Soc. Jpn. **6**, 265 (1951).
[30] A.M. Glazer and S.A. Mabud, J. Appl. Cryst. **12**, 49 (1979).
[31] J. Kobayashi, Y. Uesu, and Y. Sakemi, Phys. Rev. **B 28**, 3866 (1983).
[32] M.F. Kuprianov, S.M. Zaitsev, E.S. Gagarina, and E.G. Fesenko, Phase Trans. **4**, 55 (1983).
[33] G. Shirane, J.D. Axe, J. Harada, and J.P. Remeika, Phys. Rev. **B 2**, 155 (1970).
[34] M.D. Fontana, K. Wojcik, H. Idrissi, and G.E. Kugel, Ferroelectrics **107**, 91 (1990).
[35] R.J. Nelmes and W.F. Kuhs, Solid State Commun. **54**, 721 (1985).
[36] R.J. Nelmes, R.O. Piltz, W.F. Kuhs, Z. Tun, and R. Restori, Ferroelectrics **108**, 165 (1990).
[37] B. Rechav, N. Sicron, Y. Yacoby, B. Ravel, M. Newville, and E.A. Stern, Physica C **209**, 55 (1993).
[38] B. Ravel, E.A. Stern, Y. Yacoby, and F. Dogan, Jpn. J. Appl. Phys. **32**, 782 (1992).
[39] H. Terauchi, K. Tanabe, H. Maeda, M. Hida, N. Kamijo, M. Takashige, T. Nakamura, H. Ozawa, and R. Uno, J. Phys. Soc. Jpn. **50**, 3977 (1981).
[40] E.A. Stern and K. Kim, Phys. Rev. **B 23**, 3781 (1981).
[41] J. Mustre, Y. Yacoby, E.A. Stern, and J.J. Rehr, Phys. Rev. **B 42**, 10843 (1990).
[42] A.M. Glazer and S.A. Mabud, Acta Crystallogr. B **34**, 1065 (1978).
[43] R.E. Cohen and H. Krakauer, Ferroelectrics **136**, 65 (1992).
[44] J.J. Rehr, R.C. Albers, and S.I. Zabinsky, Phys. Rev. Lett. **69**, 3397 (1992); J.J. Rehr, S.I. Zabinski, and R.C. Albers, Phys. Rev. **B 41**, 8139 (1990).
[45] M. Newville, P. Livins, Y. Yacoby, J.J. Rehr, and E.A. Stern, Phys. Rev. **B 47**, 14126 (1993).
[46] N. Sicron, M.Sc. thesis, Hebrew University of Jerusalem, 1993.
[47] E.A. Stern, P. Livins, and Zhe Zhang, Phys. Rev. **B 43**, 8850 (1991).